Complement factor H deficiency in aged mice causes retinal abnormalities and visual dysfunction

Peter J. Coffey*, Carlos Gias*, Caroline J. McDermott†, Peter Lundh‡, Matthew C. Pickering§, Charanjit Sethi†, Alan Bird*¶, Fred W. Fitzke‡, Annelie Maass†, Li Li Chen*, Graham E. Holder¶, Philip J. Luthert†, Thomas E. Salt‡, Stephen E. Moss‖, and John Greenwood*,**

Divisions of *Cellular Therapy, †Pathology, ‡Visual Science, and ‖Cell Biology, Institute of Ophthalmology, University College London, London EC1V 9EL, United Kingdom; §Molecular Genetics and Rheumatology Section, Imperial College London, London W12 0NN, United Kingdom; and ¶Moorfields Eye Hospital, City Road, London EC1V 2PD, United Kingdom

Edited by Jeremy Nathans, Johns Hopkins University School of Medicine, Baltimore, MD, and approved August 22, 2007 (received for review June 1, 2007)

Age-related macular degeneration is the most common form of legal blindness in westernized societies, and polymorphisms in the gene encoding complement factor H (*CFH*) are associated with susceptibility to age-related macular degeneration in more than half of affected individuals. To investigate the relationship between complement factor H (CFH) and retinal disease, we performed functional and anatomical analysis in 2-year-old CFH-deficient (*cfh*$^{-/-}$) mice. *cfh*$^{-/-}$ animals exhibited significantly reduced visual acuity and rod response amplitudes on electroretinography compared with age-matched controls. Retinal imaging by confocal scanning laser ophthalmoscopy revealed an increase in autofluorescent subretinal deposits in the *cfh*$^{-/-}$ mice, whereas the fundus and vasculature appeared normal. Examination of tissue sections showed an accumulation of complement C3 in the neural retina of the *cfh*$^{-/-}$ mice, together with a decrease in electron-dense material, thinning of Bruch's membrane, changes in the cellular distribution of retinal pigment epithelial cell organelles, and disorganization of rod photoreceptor outer segments. Collectively, these data show that, in the absence of any specific exogenous challenge to the innate immune system, CFH is critically required for the long-term functional health of the retina.

age-related macular degeneration | innate immunity | retina

Age-related macular degeneration (AMD), the major cause of legal blindness in Europe, North America, and Australia (1), is a complex late-onset degenerative disease. Recently, a strong association has been described between a broad range of AMD phenotypes and polymorphisms in the gene encoding complement factor H (*CFH*), the major plasma protein regulator of the alternative pathway (AP) of complement activation (2–7). The pathological relevance of these genetic studies is supported by the demonstration that drusen, the pathogenic hallmark of AMD, contain complement proteins, including CFH (8–12). Furthermore, AMD-like changes have been described in individuals with AP dysregulation (13, 14), a phenomenon that is also associated with the inflammatory renal disease membranoproliferative glomerulonephritis type II (MPGN2). Interestingly, MPGN2 and AMD share common "at-risk" *CFH* haplotypes (5) and have pathological similarities with the accumulation of C3-containing material along the glomerular basement membrane and in drusen, respectively. Homozygous deficiency of CFH in humans (15) and mice (16) results in spontaneous MPGN2. The association between AMD-like changes and MPGN2 in humans with AP dysregulation, together with the observation that *cfh*$^{-/-}$ mice spontaneously develop MPGN2, led us to test the hypothesis that AP dysregulation due to CFH deficiency would predispose to retinopathy. To test this hypothesis, we evaluated visual function and analyzed retinal anatomy of 2-year-old C57BL/6 *cfh*$^{-/-}$ and normal age-matched control mice.

Results

CFH Deficiency Reduces Visual Acuity in Aged Mice. Animals were first tested for light–dark discrimination, visual acuity, and contrast sensitivity by using a visual water maze task (17). After initial training, visual acuity was assessed with high-contrast sinusoidal gratings, and an age-related reduction in visual acuity was observed between the young [0.44 cycles per degree (c/d)] and 2-year-old normal (0.31 c/d; ≈27%) groups of mice (Fig. 1 *A* and *B*). When visual acuity was then assessed in the 2-year-old *cfh*$^{-/-}$ mice, a further significant reduction was detected (0.29 c/d; ≈9%) compared with the age-matched controls (Fig. 1 *A* and *B*). Contrast sensitivity in the *cfh*$^{-/-}$ mice was reduced but not statistically significant (Fig. 1*C*).

CFH Deficiency Results in Rod Photoreceptor Dysfunction. Electroretinography (ERG) was used to assess retinal function in response to full-field flash stimuli under scotopic and photopic conditions. Under scotopic conditions, in which rod-mediated responses predominate, we recorded responses to light stimuli from wild-type (Fig. 1*D*) and *cfh*$^{-/-}$ (Fig. 1*E*) mice that comprised clear a- and b-wave components and oscillatory potentials on the rising slope of the b-wave. The *cfh*$^{-/-}$ animals displayed a significant ($P < 0.05$) reduction in a-wave (Fig. 1*F*) and b-wave (Fig. 1*G*) amplitudes with increasing stimulus intensity when compared with age-matched normal mice. At higher stimulus intensities (log unit 0 and +1), this was also accompanied by a reduced steepness of the initial slope of the a-wave (Fig. 1*F* *Inset*). After adaptation to photopic conditions, when responses are cone system-mediated, little difference was noted between response amplitudes or latencies of either the test or normal animals [supporting information (SI) Fig. 5 *A* and *B*]. Moreover, wild-type and *cfh*$^{-/-}$ mice exhibited a similar decline in responses with increasing frequency of flickering stimuli (up to 40 Hz) with no difference in the implicit time of the peak of the b-wave (SI Fig. 5*B*). The ERG responses of normal animals under both scotopic and photopic conditions were similar to those reported previously for aged pigmented mice (18). These data indicate that rod photoreceptor function is compromised in the *cfh*$^{-/-}$ mice, as shown by the reduction in amplitude and change in slope of the a-wave of the ERG. By contrast, the negligible difference between normal and *cfh*$^{-/-}$ mice under

Author contributions: P.J.C., A.B., F.W.F., G.E.H., P.J.L., T.E.S., S.E.M., and J.G. designed research; P.J.C., C.G., C.J.M., P.L., C.S., A.M., L.L.C., and J.G. performed research; M.C.P. contributed new reagents/analytic tools; P.J.C., C.G., C.J.M., P.L., A.B., F.W.F., G.E.H., P.J.L., T.E.S., S.E.M., and J.G. analyzed data; and M.C.P., S.E.M., and J.G. wrote the paper.

The authors declare no conflict of interest.

This article is a PNAS Direct Submission.

Abbreviations: AMD, age-related macular degeneration; AP, alternative pathway; BM, Bruch's membrane; c/d, cycles per degree; EDM, electron-dense material; ERG, electroretinography; MPGN2, membranoproliferative glomerulonephritis type II; OS, outer segment; RPE, retinal pigmented epithelium.

**To whom correspondence should be addressed. E-mail: j.greenwood@ucl.ac.uk.

This article contains supporting information online at www.pnas.org/cgi/content/full/0705079104/DC1.

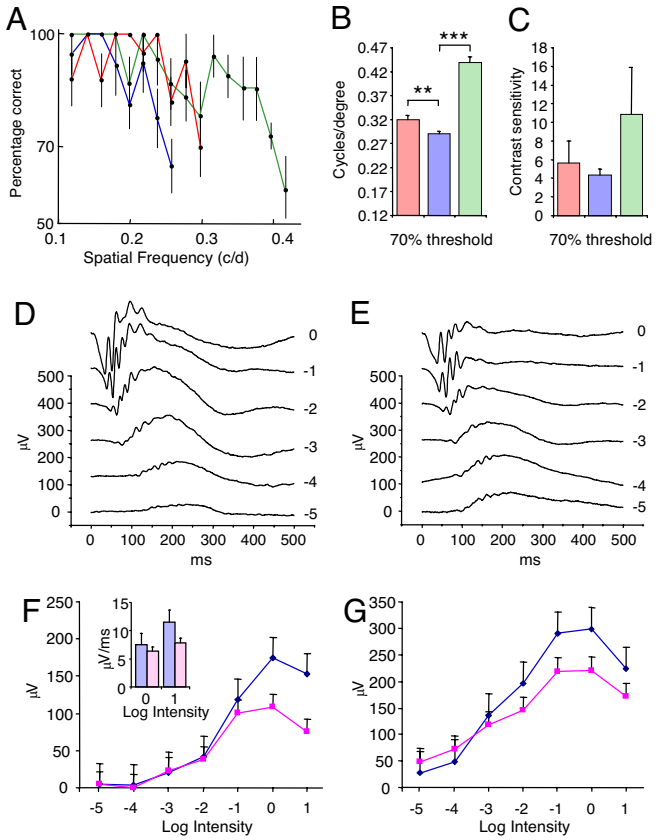

Fig. 1. Behavioral and electrophysiological assessment of retinal function in $cfh^{-/-}$ and wild-type age-matched mice. Behavioral assessment was used to evaluate visual acuity and contrast sensitivity. (*A*) Average spatial frequency performance comparison among $cfh^{-/-}$ mice (blue line, $n = 4$), age-matched controls (red line, $n = 4$), and young controls (green line, $n = 3$). Each point represents the average performance across mice for each group at a spatial frequency. Correct discrimination of large spatial frequencies, which represent narrow gratings, is indicative of high acuity. Only those spatial frequencies that were tested in every mouse within each group are represented here. Error bars represent the standard error of the mean. (*B*) Visual acuity of $cfh^{-/-}$ mice (blue bar, $n = 4$) at a 70% threshold was significantly impaired in comparison with age-matched control (red bar, $n = 4$) and young control (green bar, $n = 3$) mice. Visual acuity was determined for each individual mouse and then averaged within groups. The data represent the average acuity and standard error of the mean within each group of mice. **, significant difference as determined by ANOVA at $P < 0.05$; ***, $P < 0.001$. (*C*) Contrast sensitivity tested at 0.118 c/d at 70% threshold revealed no significant difference between the $cfh^{-/-}$ mice (blue bar, $n = 4$) and either the age-matched (red bar, $n = 3$) or young normal (green bar, $n = 3$) group ($P > 0.05$). Data represent the average contrast sensitivity and standard error of the mean within each group of mice. (*D* and *E*) ERG was used to assess scotopic neural retinal responses to flash stimuli of increasing log intensity. Representative examples of recorded evoked responses comprising clear a- and b-wave components and oscillatory potentials on the rising slope of the b-wave in wild-type (*D*, $n = 2$) and $cfh^{-/-}$ (*E*, $n = 4$) mice. (*F*) Under scotopic conditions, $cfh^{-/-}$ mice (magenta line) exhibited a significant reduction (as determined by random ANOVA; $P < 0.05$) in a-wave amplitude compared with age-matched controls (blue line). At higher stimulus intensities, the initial slope of the a-wave calculated over 5 ms also appeared to be reduced in the $cfh^{-/-}$ mice (magenta bar in *Inset*). (*G*) A reduction ($P < 0.05$) in b-wave amplitude was also seen in $cfh^{-/-}$ animals compared with wild-type controls.

photopic conditions suggests that there is minimal impairment of cone function despite occasional histological changes in the short-wavelength cone population (see below). This is in keeping with the loss of rods and rod function in AMD (19–22) and in particular impaired scotopic function in the macula (23).

CFH-Deficient Aged Mice Exhibit Increased Subretinal Autofluorescence. Using *in vivo* imaging techniques (fundus photography, reflective and autofluorescence confocal scanning laser ophthalmoscopy, and fluorescein angiography), we next investigated morphological changes in the retinas of $cfh^{-/-}$ and age-matched normal mice. Clear differences were observed in the number of autofluorescent foci in the subretinal/Bruch's membrane (BM) region (Fig. 2). These structures were visible both by 488-nm reflective (Fig. 2 *A–D*) and autofluorescence (Fig. 2 *E* and *F*) imaging, suggesting a pigmentary rather than a cellular/cytoplasmic structure. Quantitation after thresholding revealed a significant increase in the number of autofluorescent foci in the $cfh^{-/-}$ mice (Fig. 2*G*). A composite representation of autofluorescent spots across the group of $cfh^{-/-}$ animals revealed a distribution skewed toward the temporal pole (Fig. 2*H*). In AMD, localized regions of abnormally increased autofluorescence have been found by using the same form of confocal scanning laser ophthalmoscopy imaging (24). These are thought to be due to lipofuscin in the retinal pigment epithelial cell layer, the accumulation of which may impair retinal pigment epithelium (RPE) function, leading to the death of photoreceptors and visual loss. Both animal groups also exhibited inner retinal autofluorescent foci at the level of the nerve fiber layer that were in close proximity to retinal vessels (SI Fig. 6 *A–C*). Fluorescein angiography revealed no vascular leakage in either group (SI Fig. 6 *D* and *E*).

CFH-Deficient Aged Mice Have Increased C3 Deposition in the Retina. Immunohistochemical analysis of retinas from the $cfh^{-/-}$ and normal mice revealed the presence of CFH in RPE/BM of wild-type age-matched mice (SI Fig. 7*A*) that was absent in the $cfh^{-/-}$ cohort (SI Fig. 7*B*). Notably, in the complete absence of CFH, spontaneous AP activation in plasma proceeds unhindered, resulting in secondary severe fluid-phase C3 consumption. Thus, $cfh^{-/-}$ mice, in addition to developing spontaneous MPGN2, have very low plasma C3 levels (16). However, these animals have marked accumulation of C3 along the glomerular basement membrane, a lesion that is evident as early as the first week of life and precedes the morphological changes of MPGN2 (16). Immunostaining for C3 in normal animals revealed a positive signal restricted to BM with no expression in the RPE or retina (Fig. 3*A*). In the $cfh^{-/-}$ animals, C3 staining along BM was more fragmented and extended into the RPE. Moreover, the outer retina was positive for C3 with low expression along retinal vessel walls (Fig. 3*B*). The presence of C3 along the glomerular basement membrane and BM may be related to common anatomical factors: both structures, unlike cell surfaces, are devoid of intrinsic membrane-bound (but not fluid-phase) complement regulatory molecules and are lined by fenestrated endothelium allowing direct exposure to plasma C3. Hence, these sites are particularly vulnerable to plasma-derived C3 accumulation in the setting of CFH deficiency. In contrast, the presence of C3 in the neuroretina of $cfh^{-/-}$ mice suggests that local apical secretion of CFH by the RPE (25) is physiologically important in regulating retinal deposition of C3. This is likely to be especially important should there be subtle age-related breakdown of the blood–retinal barrier. Failure of such a mechanism would result in the gradual accumulation of C3 in the neuroretina with the potential for low-grade complement-mediated damage.

Retinae from CFH-Deficient Mice Exhibit Stress-Related Responses. We next tested whether the accumulation of C3 may result in retinal stress. Although short-wavelength cone opsin was localized predominantly to the outer segments (OSs) of age-matched control animals (Fig. 3*C*), in $cfh^{-/-}$ animals, there was a greater redistribution of protein to more proximal cell compartments, in some cases outlining the entire cell (Fig. 3*D*). Redistribution of

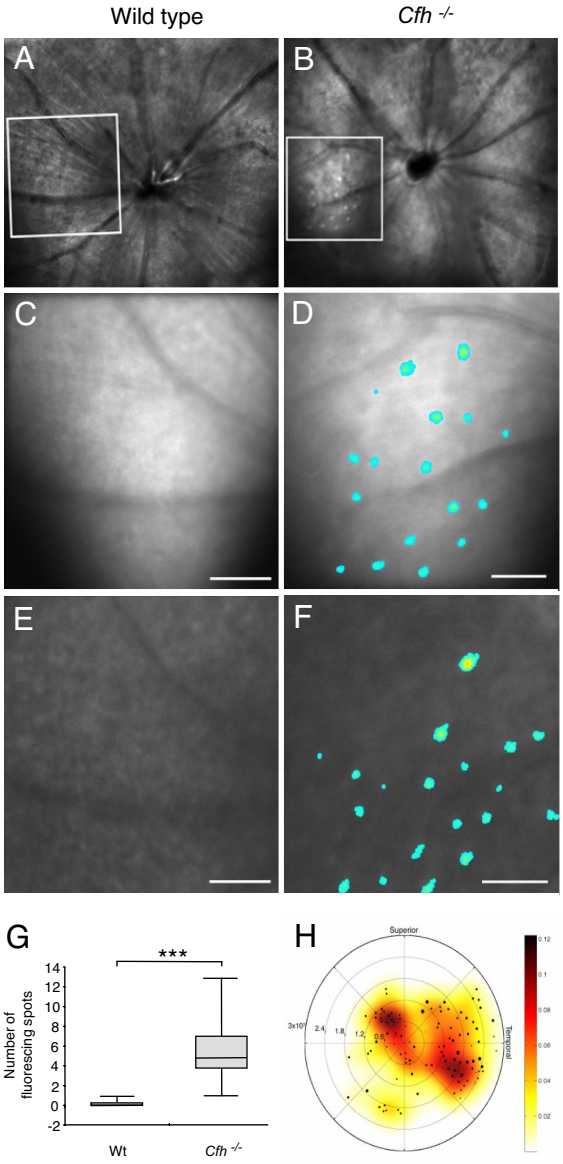

Fig. 2. Accumulation of autofluorescent deposits in mice lacking CFH. (*A* and *B*) Representative *in vivo* confocal 488-nm reflectance images. (*C–F*) Expanded reflectance (*C* and *D*) and autofluorescence (*E* and *F*) images of the boxed regions in *A* and *B* recorded at the level of the retinal pigment epithelium of wild-type age-matched control (*A*, *C*, and *E*, $n = 5$) and $cfh^{-/-}$ (*B*, *D*, and *F*, $n = 4$) mouse fundus. The expanded images show typical clusters of autofluorescent deposits that are lacking in the age-matched controls. Thresholding and pseudocolor are used to highlight the presence of autofluorescent structures. (Scale bars: 500 μm.) (*G*) The box plots represent the number of subretinal autofluorescent structures in $cfh^{-/-}$ and wild-type age-matched control mice at the level of the RPE and demonstrate a significantly greater number of subretinal autofluorescent deposits ($t = 1.64$, df = 3, and $P = 0.046$) at the RPE level in $cfh^{-/-}$ mice. (*H*) A composite of all autofluorescent deposits in $cfh^{-/-}$ retinas ($n = 4$) is plotted in a polar coordinate system centered on the optic disk of the mouse and reveals an increased density of subretinal autofluorescent deposits in the superior and temporal areas of the retina. Eccentricity from the optic disk is measured in millimeters, and the polar angle corresponds to the retinal direction. Marker sizes corresponding to the diameter of each fluorescent point are superimposed over a pseudocolored surface representing the smoothed density of all points. The color bar indicates the normalized density values.

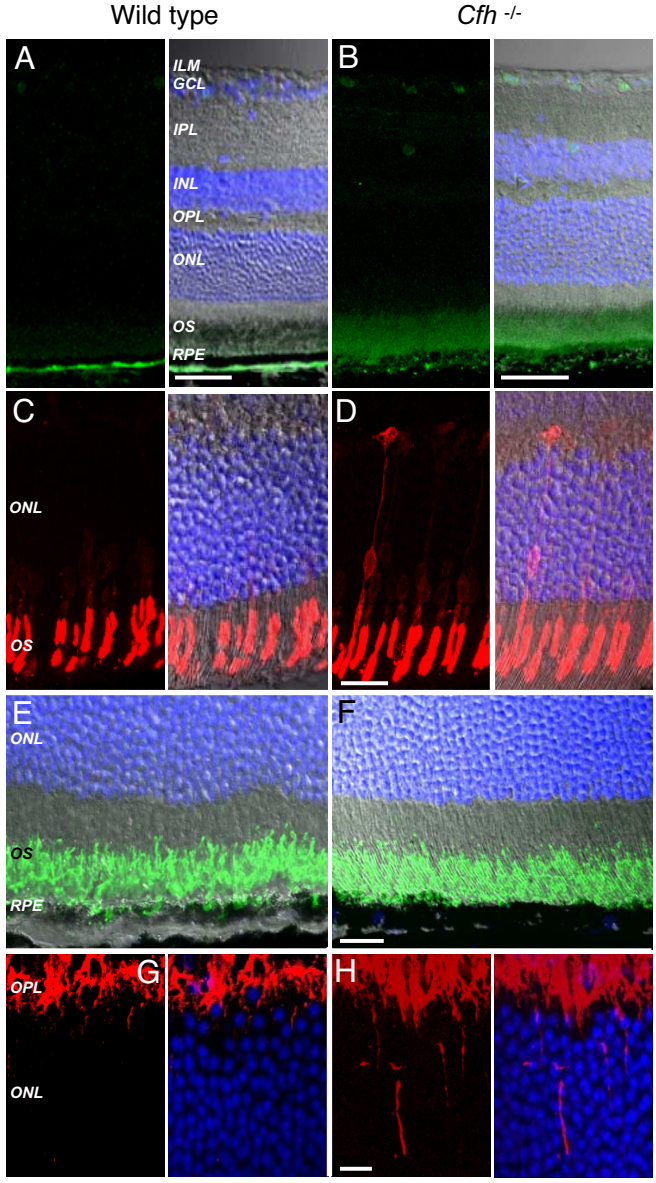

Fig. 3. Immunohistochemical analysis of retinas from $cfh^{-/-}$ and wild-type age-matched control mice. Shown are representative images from wild-type age-matched control ($n = 3$) and $cfh^{-/-}$ ($n = 4$) mice. (*A*) In control mice, complement C3 (green) is detectable at the level of BM below the RPE and is absent from the neuroretina. (*B*) In $cfh^{-/-}$ mice, C3 is present in BM but also extends into the RPE and is expressed in the OSs and surrounding retinal vessels. (Scale bars: 50 μm.) (*C* and *D*) Blue cone opsin (red) in normal animals is distributed normally within the OS layer of the photoreceptors (*C*) but can be observed extending into the outer nuclear layer in $cfh^{-/-}$ mice (*D*). (Scale bar: 20 μm.) (*E* and *F*) In control (*E*) and $cfh^{-/-}$ (*F*) mice, rod opsin (green) was observed to be correctly localized to the photoreceptor OS. (Scale bar: 20 μm.) (*G*) PKC (red), which is expressed by retinal bipolar cells, can be seen staining the outer plexiform layer in wild-type animals. (*H*) In $cfh^{-/-}$ mice, PKC-positive cell extensions are observed entering further into the outer nuclear layer. (Scale bar: 10 μm.) Nuclei are stained blue with DAPI. ILM, inner limiting membrane; GCL, ganglion cell layer; IPL, inner plexiform layer; OPL, outer plexiform layer; ONL, outer nuclear layer.

short-wavelength cone opsin in this manner has previously been reported in photoreceptor cells undergoing degenerative changes, and the labeling of the entire cell for opsin is also a feature of early human retinal detachment (26) as well as other retinal degenerations. Rod opsin was distributed normally in the OSs in both knockout (Fig. 3*E*) and wild-type (Fig. 3*F*) mice. Protein kinase C labeling revealed rod bipolar cells with occasional fine dendrites sprouting into the outer nuclear layer of normal animals (Fig. 3*G*), but these extensions were more

prominent and numerous in the $cfh^{-/-}$ group (Fig. 3*H*). Extension of bipolar cell dendrites into the outer nuclear layer is a recognized feature of clinical and experimental retinal degeneration (26, 27), and it has been suggested that as axon terminals withdraw to the cell bodies in stressed photoreceptors, second-order neurons respond by extending processes in an attempt to maintain synaptic and trophic contact. The presence of C3 in the neuroretina is likely to result in immune-mediated damage to the retina and in the functional changes observed in this study. Despite these changes in $cfh^{-/-}$ mice, no significant reduction in the number of photoreceptor cell nuclear profiles was found [$1.40 \pm 0.12 \times 10^3$ mm^{-1} in controls ($n = 3$) versus $1.36 \pm 0.12 \times 10^3$ mm^{-1} in $cfh^{-/-}$ animals ($n = 3$)].

CFH-Deficient Aged Mice Display Ultrastructural Changes to the Retina. Next, we undertook a detailed ultrastructural examination of the retinas from wild-type control and $cfh^{-/-}$ mice. Toluidine blue-stained semithin resin sections revealed normal histology for both groups of animals with the exception of the $cfh^{-/-}$ mice, which exhibited a greater preponderance of retinal detachment, of uncertain significance, during processing (Fig. 4 *A* and *B*). Ultrastructurally, however, we observed a significant decrease in the amount of sub-RPE electron-dense material (EDM) in the $cfh^{-/-}$ mice in comparison with normal mice ($P < 0.001$; Fig. 4 *C–E*). Because the imaging data (Fig. 2) revealed an increase in fluorescent structures, it is likely that the EDM and fluorescent deposits consist of different material and are produced and removed by separate mechanisms. In addition, a significant decrease (29%) in BM thickness was also seen in the $cfh^{-/-}$ mice when compared with normal mice ($P < 0.001$; Fig. 4*F*). In AMD, both BM thickening and increased EDM are observed. In contrast, our data suggest that CFH deficiency is associated with a net reduction of EDM that is associated with a decrease in BM thickness. The mechanism of EDM turnover is not defined, but we hypothesize that EDM may be removed by phagocytosis through a "waste disposal" mechanism. In $cfh^{-/-}$ mice, uncontrolled C3 activation on EDM may paradoxically potentiate phagocytic uptake. Alternatively, CFH may be a key component of sub-RPE deposits, and in its absence, rate of deposition is slowed. Nevertheless, the increased presence of C3 within the neuroretina may result in concomitant damage.

Discrete regions of misaligned, disorganized photoreceptor OSs were consistently observed in the $cfh^{-/-}$ mice (Fig. 4*D*) when compared with age-matched normal mice (Fig. 4*C*). In these areas, the interface between the RPE cell and the OS was abnormal with loss of the intimate relationship between the perpendicular OS tips and apical microvilli of the RPE. Many OSs were bent, and some were lying horizontally along the apical aspect of the RPE. These abnormalities are consistent with the recorded changes in visual function. Similar OS changes have been reported in donor eyes from elderly humans and were interpreted as reflecting an imbalance between OS formation and shedding/phagocytosis (28). The distribution of organelles within the RPE layer was also significantly different between the two groups of mice ($P < 0.0001$; Fig. 4 *C*, *D*, and *G*) even though there was no significant difference between the height of RPE cells (≈ 9 μm). In the $cfh^{-/-}$ mice, the organelles were dispersed throughout the RPE, whereas in the controls, they were concentrated toward the apical aspect of the cell. The apical location, especially of melanin granules, under normal conditions may provide a protective role, and focal loss of organelle polarity can be observed in human RPE from elderly individuals.

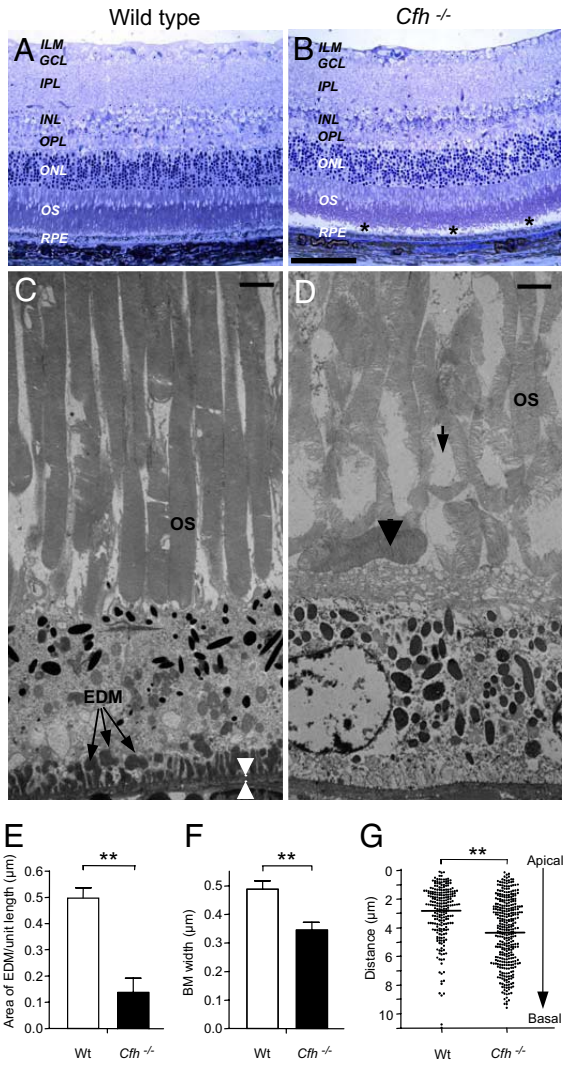

Fig. 4. Ultrastructural analysis of subretinal region of aged $cfh^{-/-}$ and wild-type mice. (*A* and *B*) Representative toluidine blue-stained semithin resin section of wild-type age-matched control (*A*, $n = 3$) and $cfh^{-/-}$ (*B*, $n = 3$) mouse retina. Postprocessing detachment of the retina is indicated by asterisks. (Scale bar: 100 μm.) ILM, inner limiting membrane; GCL, ganglion cell layer; IPL, inner plexiform layer; OPL, outer plexiform layer; ONL, outer nuclear layer. (*C*) Representative transmission electron micrograph of wild-type age-matched control animal, showing abundant EDM (arrows) between the basal RPE and BM (region between arrowheads). (Scale bar: 2 μm.) (*D*) Less EDM was present in the $cfh^{-/-}$ mice. (Scale bar: 2 μm.) $cfh^{-/-}$ sections exhibited discrete regions of abnormal photoreceptor OS with a loss of the normal relationship between OS tips and apical microvilli of the RPE. OSs were frequently disorganized (arrow) and bent, lying along the apical aspect of the RPE (arrowhead). The $cfh^{-/-}$ animals also exhibited a thinner BM and greater number of RPE organelles, which extended more basally. (*E* and *F*) Quantification of these parameters revealed a significant reduction in both the surface area of EDM (*E*) and BM thickness (*F*) in the $cfh^{-/-}$ mice (**, $P < 0.001$). (*G*) The distribution of melanosomes, lipofuscin granules, and melanosome-lipofuscin granules within the RPE of $cfh^{-/-}$ mice was also altered significantly (**, $P < 0.001$), as shown by the scatter plot, where each dot represents an individual structure and its distance from the RPE apical surface.

Discussion

Together, these *in vivo* data demonstrate that CFH is critically required for the long-term health of the murine retina. Thus, in the absence of CFH, we observed ERG anomalies and an increase in subretinal fluorescent material. Moreover, CFH deficiency was associated with C3 deposition within the neuroretina that may be derived from systemic sources, due to increased leakage of the posterior blood–retinal barrier, or possibly from local production (8). Furthermore, we have shown that even with a lack of a direct immune challenge, retinal damage occurs in the absence of CFH. This suggests that complement-mediated retinal disease may occur

without the need for an environmental infectious "trigger," a notion supported by the recent report that lipofuscin derivatives alone are sufficient to activate the complement pathway (29). Although we did not observe quantifiable photoreceptor cell loss, it is possible that changes to the extracellular environment, such as an increase in C3 deposition, will affect photoreceptor transduction efficiency.

Unexpectedly, the absence of CFH resulted in a reduction in BM thickness and EDM deposition. This may be explained by the dual role of complement in possessing both beneficial and pathologic functions (30). Thus, uncontrolled C3 activation may result in neuronal damage on the one hand while stimulating the subretinal debris clearance mechanisms on the other (31). Our study therefore demonstrates that homozygous CFH deficiency reproduces some but not all of the hallmarks of AMD. This may be due to the *cfh* polymorphism possessing altered (as opposed to a loss of) function, but factors such as species differences in the innate immune system, the absence of a macula, or the lack of additional stressors such as infection may also prohibit the development of an AMD phenotype in the mouse. A major difference between the *cfh* polymorphisms associated with human AMD and homozygous deficiency of CFH is that in the latter, plasma C3 levels are markedly reduced, while in the former, they are normal. Secondary C3 deficiency may critically influence the ocular phenotype described in the $cfh^{-/-}$ mice. For example, C3a blockade ameliorated vascular proliferation in a murine choroidal neovascularization model (32).

The functional significance of the AMD at-risk *CFH* polymorphisms is not understood. The CFH^{Y402H} polymorphism is associated with reduced heparin binding that may impair targeting of CFH to sites of complement activation (33). However, this does not explain the molecular pathogenesis of other AMD at-risk *CFH* polymorphisms such as CFH^{I62V} or the protective *CFH* haplotype associated with deletion of FHR1 and FHR3 (34). Our data demonstrate that uncontrolled AP activation in the setting of murine CFH deficiency results in spontaneous retinal changes in aged animals. This is consistent with the hypothesis that AMD at-risk *CFH* polymorphisms are likely to be associated with enhanced AP activation, a finding supported by the recent association of AMD with protective haplotypes in the *C2/BF* locus that is postulated to result in reduced AP activation (35). Moreover, it has now been shown that a common polymorphism in the human *C3* gene strongly associates with AMD (36). The authors speculate that the Arg80Gly polymorphism may weaken a potential interaction with CFH that, in turn, would lead to impaired regulation of C3 activation. A role for C3 activation in AMD has also been suggested because increased plasma C3a des Arg levels, a surrogate marker of complement activation, have been reported in AMD patients but without correlation to the at-risk *CFH* haplotypes (37).

In conclusion, our data provide *in vivo* evidence that CFH deficiency is associated with spontaneous retinal changes and also provide mechanistic insights into the relationship between CFH dysfunction and human AMD. Furthermore, they imply that abnormalities of the AP due to base changes in CFH may cause pathology that is not limited to BM.

Materials and Methods

Animals. Two-year-old $cfh^{-/-}$ mice ($n = 5$; backcrossed onto the C57BL/6 genetic background for 10 generations) and age-matched normal C57BL/6 mice ($n = 5$) were fed lab chow ad libitum and housed in a temperature-controlled environment with a 12-h day (160 lux)–night cycle. All experimental procedures complied with and were carried out under the United Kingdom Animals (Scientific Procedures) Act 1986.

Acuity and Contrast Sensitivity Measurements. Acuity and contrast sensitivity were assessed in $cfh^{-/-}$ mice ($n = 4$), age-matched wild-type control mice ($n = 4$), and 2-month-old 129/SV control mice ($n = 3$) by using a visual water maze task (17). For further details, see *SI Materials and Methods*.

Visual acuity was evaluated by training the mice to discriminate a 0.118 c/d vertical sinusoidal grating from a uniform gray level of equal average luminance. During testing, the spatial frequency was gradually increased until visual discrimination fell below 70%. In the low-frequency range (0.118 to <0.250 c/d), after a correct choice, one sine wave cycle was added to the grating on the next trial. In the medium-frequency range (>0.250 to <0.375 c/d), three consecutive correct trials were required before increasing the spatial frequency, whereas four consecutive correct trials were required in the high-frequency range (>0.375 c/d). The initial visual threshold was estimated as the spatial frequency at which the animal's discrimination fell below 70%. The highest visual threshold at the 70% level between the two measurements was taken as the visual acuity of the animal. Statistical differences between groups were evaluated by using ANOVA.

Contrast sensitivity was tested at 0.118 c/d, starting from the maximum possible contrast (>99%). Contrast was then reduced in consecutive steps. The initial visual threshold was first estimated as the contrast at which the animal's discrimination fell below 70%. A second run was then carried out, starting at a grating with a contrast three steps above the threshold. The lowest contrast below the 70% level between the two runs was chosen as the contrast threshold. Statistical differences between groups were evaluated by using ANOVA.

ERG. $cfh^{-/-}$ ($n = 4$) and age-matched control ($n = 2$) mice were dark-adapted overnight before ERG. ERG was carried out under scotopic conditions by subjecting the animals to flash stimuli (10 μs to 1 ms in duration, repetition rate of 0.1–1 Hz; log intensity of -5 to $+1$). After completion of the scotopic series, mice were adapted to a 20 cd/m^2 background for 20 min, after which photopic responses to flash stimuli and flicker stimuli (up to 40 Hz) were assessed. Statistical differences between groups were evaluated by using random ANOVA (see *SI Materials and Methods*).

Retinal Imaging. Imaging was performed on 2-year-old $cfh^{-/-}$ ($n = 4$) and age-matched control ($n = 5$) mice as described in detail in *SI Materials and Methods*. Pupils were dilated, and color fundus photography was taken. High-resolution and high-contrast retinal images were acquired with a confocal scanning laser ophthalmoscope as described in *SI Materials and Methods*. Briefly, reflectance imaging was performed by using 488- and 820-nm laser lines. Autofluorescence and fluorescein angiography images of the mouse retina were recorded by using 488-nm excitation and the built-in standard emission cut-off filter with the edge of the barrier (value of 50% transmission) at 498 nm. Mice were injected i.p. with sodium fluorescein, and image sequences of 125 fluorescence images were captured and averaged. Tomographic image stacks were made of the retina, where the focused plane was sequentially moved, at 15-μm intervals, vitreous to sclera. Differences between the $cfh^{-/-}$ and age-matched control animals in the number of subretinal autofluorescent deposits at the level of the RPE were analyzed by applying the Student unpaired *t* test.

Histology and Immunohistochemistry. Animals were deeply anesthetized with pentobarbitone and then perfused with 0.1 M PBS, followed by 4% paraformaldehyde (in 0.1 M PBS, pH 7.4). Eyes were removed and placed in 4% paraformaldehyde before cryoprotection in 30% sucrose solution (in 0.1 M PBS buffer) and left for 24 h at 4°C. The lens was removed through a corneal incision, and the eyes were rapidly frozen in OCT compound and sectioned at a thickness of 20 μm for immunohistochemical analysis (see *SI Materials and Methods*). Tissue sections from $cfh^{-/-}$ ($n = 4$) and

age-matched control ($n = 3$) mice were incubated with antibodies raised against glial fibrillary acidic protein, rod opsin, blue cone opsin, protein kinase Cα, CFH, and C3 followed by appropriate fluorescently conjugated secondary antibodies and DAPI to stain the nuclei. For further details, see *SI Materials and Methods*. Sections were viewed on a laser scanning confocal microscope (LSM 510; Zeiss, Thornwood, NY).

Ultrastructural Analysis. Eyes from *cfh*$^{-/-}$ ($n = 3$) and age-matched control ($n = 3$) animals were immersion-fixed and prepared for transmission electron microscopy, and images were captured as described in detail in *SI Materials and Methods*. From these images, we determined the thickness of BM, the amount of EDM, and the number and distribution of melanosomes, lipofuscin granules, and melanosome-lipofuscin in the RPE. As appropriate, a Mann–Whitney *U* test or Student *t* test was used to assess significance of any differences between the two sets of animals.

We thank Dr. Peter Munro for technical expertise in the microscopic analysis of the tissue.

1. Smith W, Assink J, Klein R, Mitchell P, Klaver CCW, Klein BEK, Hofman A, Jensen S, Wang JJ, de Jong PTVM (2001) *Ophthalmology* 108:697–704.
2. Haines JL, Hauser MA, Schmidt S, Scott WK, Olson LM, Gallins P, Spencer KL, Kwan SY, Noureddine M, Gilbert JR, *et al.* (2005) *Science* 308:419–421.
3. Edwards AO, Ritter R, III, Abel KJ, Manning A, Panhuysen C, Farrer LA (2005) *Science* 308:421–424.
4. Klein RJ, Zeiss C, Chew EY, Tsai J-Y, Sackler RS, Haynes C, Henning AK, San Giovanni JP, Mane SM, Mayne ST, *et al.* (2005) *Science* 308:385–389.
5. Hageman GS, Anderson DH, Johnson LV, Hancox LS, Taiber AJ, Hardisty LI, Hageman JL, Stockman HA, Borchardt JD, Gehrs KM, *et al.* (2005) *Proc Natl Acad Sci USA* 102:7227–7232.
6. Zareparsi S, Branham KEH, Li M, Shah S, Klein RJ, Ott J, Hoh J, Abecasis GR, Swaroop A (2005) *Am J Hum Genet* 77:149–153.
7. Thakkinstian A, Han P, McEvoy M, Smith W, Ho J, Magnusson K, Zhang K, Attia J (2006) *Hum Mol Genet* 15:2784–2790.
8. Mullins RF, Russell SR, Anderson DH, Hageman GS (2000) *FASEB J* 14:835–846.
9. Hageman GS, Luthert PJ, Chong NHV, Johnson LV, Anderson DH, Mullins RF (2001) *Prog Retinal Eye Res* 20:705–732.
10. Johnson LV, Leitner WP, Staples MK, Anderson DH (2001) *Exp Eye Res* 73:887–896.
11. Crabb JW, Miyagi M, Gu X, Shadrach K, West KA, Sakaguchi H, Kamei M, Hasan A, Yan L, Rayborn ME, *et al.* (2002) *Proc Natl Acad Sci USA* 99:14682–14687.
12. Anderson DH, Mullins RF, Hageman GS, Johnson LV (2002) *Am J Ophthalmol* 134:411–431.
13. Duvall-Young J, MacDonald MK, McKechnie NM (1989) *Br J Ophthalmol* 73:297–302.
14. Leys A, Vanrenterghem Y, Van Damme B, Snyers B, Pirson Y, Leys M (1991) *Graefes Arch Clin Exp Ophthalmol* 229:406–410.
15. Levy M, Halbwachs-Mecarelli L, Gubler MC, Kohout G, Bensenouci A, Niaudet P, Hauptmann G, Lesavre P (1986) *Kidney Int* 30:949–956.
16. Pickering MC, Cook HT, Warren J, Bygrave AE, Moss J, Walport MJ, Botto M (2002) *Nat Genet* 31:424–428.
17. Prusky GT, Douglas RM (2003) *Eur J Neurosci* 17:167–173.
18. Gresh J, Goletz PW, Crouch RK, Rohrer B (2003) *Visual Neurosci* 20:211–220.
19. Chen J, Fitzke F, Pauliekhoff D, Bird AC (1992) *Invest Ophthalmol Visual Sci* 33:334–340.
20. Curcio CA, Medeiros NE, Millican CL (1996) *Invest Ophthalmol Visual Sci* 37:1236–1249.
21. Feigl B, Brown B, Lovie-Kitchin J, Swann P (2005) *Eye* 19:431–441.
22. Jackson GR, McGwin G, Jr, Phillips JM, Klein R, Owsley C (2006) *Vision Res* 46:1422–1431.
23. Scholl HP, Bellmann C, Dandekar SS, Bird AC, Fitzke FW (2004) *Invest Ophthalmol Visual Sci* 45:574–583.
24. Von Ruckmann A, Fitzke FW, Bird AC (1997) *Invest Ophthalmol Visual Sci* 38:478–486.
25. Chen M, Forrester JV, Xu H (2007) *Exp Eye Res* 84:635–645.
26. Sethi CS, Lewis GP, Fisher SK, Leitner WP, Mann DL, Luthert PJ, Charteris DG (2005) *Invest Ophthalmol Visual Sci* 46:329–342.
27. Lewis GP, Linberg KA, Fisher SK (1998) *Invest Ophthalmol Visual Sci* 39:424–434.
28. Marshall J, Grindle J, Ansell PL, Borwein B (1979) *Br J Ophthalmol* 63:181–187.
29. Zhou J, Jang YP, Kim SR, Sparrow JR (2006) *Proc Natl Acad Sci USA* 103:16182–16187.
30. Walport MJ (2001) *N Engl J Med* 344:1058–1066.
31. Walport MJ (2001) *N Engl J Med* 344:1140–1144.
32. Nozaki M, Raisler BJ, Sakurai E, Sarma JV, Barnum SR, Lambris JD, Chen Y, Zhang K, Ambati BK, Baffi JZ, *et al.* (2006) *Proc Natl Acad Sci USA* 103:2328–2333.
33. Clark SJ, Higman VA, Mulloy B, Perkins SJ, Lea SM, Sim RB, Day AJ (2006) *J Biol Chem* 281:24713–24720.
34. Hughes AE, Orr N, Esfandiary H, Diaz-Torres M, Goodship T, Chakravarthy U (2006) *Nat Genet* 38:1173–1177.
35. Gold B, Merriam JE, Zernant J, Hancox LS, Taiber AJ, Gehrs K, Cramer K, Neel J, Bergeron J, Barile GR, *et al.* (2006) *Nat Genet* 38:458–462.
36. Yates JR, Sepp T, Matharu BK, Khan JC, Thurlby DA, Shahid H, Clayton DG, Hayward C, Morgan J, Wright AF, *et al.* (2007) *N Engl J Med* 357:553–561.
37. Sivaprasad S, Adewoyin T, Bailey TA, Dandekar SS, Jenkins S, Webster AR, Chong NV (2007) *Arch Ophthalmol* 125:515–519.